Journal of Ceramic Processing Research. Vol. 11, No. 2, pp. 241~249 (2010)

J O U R N A L O F
Ceramic Processing Research

Electrical and magnetic properties of rare earth substituted strontium hexaferrites

Anterpreet Singh[a,*], S. Bindra Narang[b], Kulwant Singh[c], O.P. Pandey[d] and R.K. Kotnala[e]

[a]*Department of Physics, Baba Kuma Singh Ji Engineering College, Amritsar, India*
[b]*Department of Electronics Technology, Guru Nanak Dev University, Amritsar, India*
[c]*Department of Physics, Guru Nanak Dev University, Amritsar, India*
[d]*School of Physics and Materials Science, Thapar University, Patiala, India*
[e]*Magnetic Materials & Standards, National Physical Laboratory, New Delhi, India*

Samples of strontium ferrite (Sr-M) with different molar substitution concentrations of lanthanum, neodymium and samarium ions were prepared by a standard ceramic processing technique. AC conductivity, dielectric constant and dielectric loss tangent measurements were carried out in the frequency range of 20 Hz to 1 MHz. The experimental results indicate that AC electrical conductivity increases with increasing frequency. The increase in AC conductivity with frequency can be explained on the basis of Koops model, whereas the dielectric constant and dielectric loss tangent variations have been explained with a Maxwell-Wagner type interfacial polarization in agreement with the Koops phenomenological theory. The effects of rare earth substitution on the magnetic properties such as the saturation magnetization moment (M_s), coercive field (H_c), remenance (M_r), and Curie temperature T_c (K) have been investigated. It is found that the values of the magnetization moment (M_s), and remenance (M_r) decrease with increasing rare earth ions substitution for all the series. The reason for the decrease may be both the magnetic dilution and spin canting, which promote reduction of superexchange interactions. The enhancement of H_c values may be due to higher magnetocrystalline anisotropy, where Fe^{2+} ion anisotropy on the 2a site could be dominant in all hexaferrites series.

Key words: Hexagonal ferrites, AC conductivity, Dielectric constant, Dielectric loss tangent and Magnetic measurements.

Introduction

M-type hexagonal ferrites having the general formula $MFe_{12}O_{19}$ (where M is Sr, Ba or Pb) are hard magnetic materials with a magnetoplumbite structure. Because of the fact, that strontium ferrite has a low price per unit available magnetic energy, this material continues to occupy an importance particular in the permanent magnets market. This material is chemically stable and once known for its high uniaxial magnetocrystalline anisotropy with an easy axis of magnetization along the hexagonal c-axis [1]. When compared with alnico-magnets, strontium ferrite has high coercivity (240-340 k A/m), moderate remenance (≈350 mT), excellent chemical stability and corrosion resistance [2, 3].This material is being used in bulk form in many electrical and electronic devices due to its better magnetic properties, such as in microwave devices, small motors, and, more recently, magnetic recording applications. In order to improve the magnetic properties of strontium hexaferrites, many studies have also been carried out with cationic substitutions [4]. Some researchers have used rare earth and other metal cations substitution for Ba, Sr and Fe, respectively, taking into account the ionic radius of the element substituted [5].

The hexagonal ferrite crystallizes in a hexagonal symmetry with space group $P6_3/mmc$ in which the iron ions are coordinated tetrahedrally (FeO_4), trigonal bipyramidally (FeO_5) and octahedrally (FeO_6) by oxygen ions. The structure comprises 64 ions per hexagonal unit cell on 11 distinct basic sites. The 24 Fe^{3+} ions are distributed on five different crystallographic sites: three octahedral sites (12k, 2a, and 4f2), one tetrahedral site (4f1) and one trigonal bipyramidal site (2b) [6, 7]. The ferromagnetic structure given by the Gorter model shows, three parallel (12k, 2a, and 4f2) and two anti-parallel (4f1 and 4f2) sites, which are coupled by super- exchange interactions through the O^{2-} ions [6]. One group has reported the enhancement in its magnetic properties by varying the processing conditions (mole ratio, calcination temperature and sintering temperature etc.) thereby improving its microstructural features [8, 9]. While, another group of researchers have concentrated their studies on partial substitution of divalent-tetravalent ions such as Ni-Ti, Co-Ti, Bi-Co etc. [10-12] as well as trivalent metal ions such as Al, Cr, Bi and La etc.[13, 14] and observed a variation in magnetic properties of strontium ferrite sintered magnets. Many reports have recently shown that rare earth (RE) substituted M-type hexaferrites have improved magnetic properties [15-17]. The improvement is largely associated with the increase of both magnetocrystalline anisotropy and coercive field with magnetization [15, 17].

*Corresponding author:
Tel : +91-183-2384311
Fax: +91-183-2384314
E-mail: apsingh_76@ yahoo.co.in

Effects have also been made to enhance physical properties of $SrFe_{12}O_{19}$ with pair doping such as La-Co pairs to replace Sr-Fe pairs [18, 19]. Apart from magnetic properties, electrical properties of these ferrites are very sensitive to the processing conditions and type of substitution. Also it is known that the electrical properties of ferrites are derived from many physical and chemical characteristics. The dielectric behavior offers much valuable information about the localized charge carriers which depend upon the composition of the ferrite and also varies with frequency and temperature of operation. Studies of such variations help to elucidate the mechanisms responsible for charge transport phenomena and dielectric behavior. Many researchers have studied the dielectric and electrical properties of different hexaferrites [20, 21]. However, investigations of the substitutional effect on the electrical and dielectric properties of strontium ferrite are rare.

Since strontium ferrite has higher magnetocrystalline anisotropy as compared to Ba and Pb ferrites, efforts have been made in the present investigation to study the effect of rare earth ions substitution on the electrical and magnetic properties of strontium ferrites which were prepared by a ceramic processing technique. The effect of rare earth substitution (La^{3+}, Nd^{3+} and Sm^{3+}) on the electrical and magnetic properties such as AC conductivity (σ_{AC}), dielectric constant (ε'), dielectric loss tangent (tan δ), saturation magnetization (M_s), coercive field (H_c)and remenance (M_r) have been studied in detail.

Experimental

A series of $Sr_{1-x}RE_xFe_{12}O_{19}$ samples with different substitution ratios were prepared by a standard ceramic processing technique. High purity precursors $SrCO_3$ (99% purity), RE_2O_3 (99.9% purity) and Fe_2O_3 (97% purity) were mixed together in the appropriate molar ratio, calculated from the following chemical reaction:

$$(1-x)\ SrCO_3 + 6Fe_2O_3 + (x/2)\ RE_2O_3 \rightarrow Sr_{1-x}RE_xFe_{12}O_{19} + (1-x)\ CO_2 + (x/4)\ O_2 \quad (1)$$

where, x varies from 0 to 0.30 with an increment of 0.10. The details of the preparation method have been given in our earlier publications [22, 23]. But in brief the appropriate quantities of powders were weighed and wet mixed in distilled water and milled for 6 hours in an agate mortar and pestle fitted with an electric grinder rotating at a speed of 100 rpm. After milling, the dried powders were calcined at 1200 °C for six hours. The calcined powders were further wet-milled in distilled water for 8 hours to obtain very fine and uniform size powders. After milling, the powders were again dried and 5% polyvinyl alcohol was added to them, which acts as a binder. These materials were then granulated through sieves of 60-80 mesh B.S.S (250-180 μm approximately). The granules were cold pressed in a die at a compressed load of 75 kN to produce pellets of 14.5 mm diameter and 3.0 mm to 4.0 mm thickness. These pellets were finally sintered at 1250 °C for 2 h. The phase analysis of these sintered pellets was carried out by an X-ray diffractometer (Model RIGAKU D- MAX III C). The microstructural studies of the samples were carried out by a scanning electron microscope (Model JEOL 6100). AC conductivity and dielectric measurements of all ferrite samples were done in the frequency range from 20 Hz-1 MHz using a precision inductance capacitance resistance meter (Model HP4284A) by a standard two-probe technique using platinum electrodes. The AC conductivity was determined using the formula:

$$\sigma_{AC} = \frac{Gt}{A} \quad (2)$$

where t and A are the thickness and cross-sectional area of pellets and G is the conductance.

The value of the dielectric constant (ε') of the ferrite samples can be calculated using the formula:

$$\varepsilon' = \frac{C_{pt}}{\varepsilon_a A} \quad (3)$$

where C_p is the capacitance of samples in pF, t the thickness of the samples in cm, A is the cross-sectional area of the sample in cm^2 and ε_0 is the permittivity in free space having a value 8.854×10^{-2} pF/cm. The magnetization measurements of all samples were carried out by a vibrating sample magnetometer (Model LAKESHORE 7306).

Results and Discussion

Structural Analysis

X-Ray diffraction

Fig. 1 shows a sequence of X-ray diffraction pattern obtained at different molar concentrations of $Sr_{1-x}RE_xFe_{12}O_{19}$ (RE = La^{3+}, Nd^{3+} and Sm^{3+}). The analysis reveals that in the case of the La^{3+} substitution, the samples are a single hexagonal M-type phase (Fig. 1a). No peaks of Fe_2O_3 and La_2O_3 phases are observed, which suggests that Sr^{2+} ions are substituted by La^{3+} ions [17]. In the case of the Nd^{3+} series all peaks correspond to hexaferrites. However, in the case of $Nd^{3+} = 0.30$, there is an extra peak for hematite (Fig. 1b (0.30)). No peak of Nd_2O_3 is observed. This suggests that Nd^{3+} is completely substituting for Sr. The existence of the hematite peak for the substitution x = 0.30 is because of unreacted Fe_2O_3 which may be because of improper heat treatment. In the case of the Sm^{3+} series all peaks correspond to hexaferrites, however in the case of $Sm^{3+} = 0.30$ there are extra peaks of hematite and tetragonal $Sr_3Fe_2O_7$ which are observed (Fig. 1c). No $SmFeO_3$ phase is observed. The emergence of these extra phases may be due to partial substitution of Sm^{3+} for Sr^{2+} in the M-type ferrite structure. This substitution causes an excess of Sr^{2+}, which favours the stochiometry for the formation of these secondary phases. Since sintering of all samples was done at 1250 °C to make a better comparison so the possibility exists that iron oxide may not find the required activation energy to migrate into interstitial sites. However, in the case of the Sm^{3+} substitution, $Sr_3Fe_2O_7$

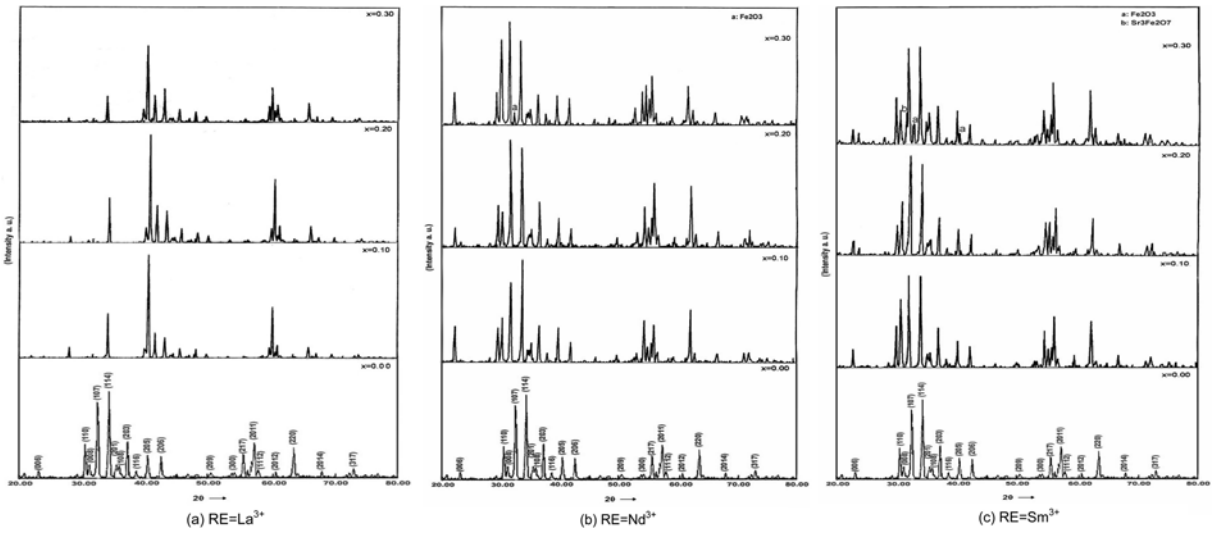

Fig.1. X-ray diffraction pattern for the $Sr_{1-x}RE_xFe_{12}O_{19}$ where RE = La^{3+}, Nd^{3+} and Sm^{3+} with (x = 0 to 0.30) for La^{3+} (a), Nd^{3+} (b) and Sm^{3+} (c) respectively.

and the hematite phase appear because of lattice straining. But no peak of $SmFeO_3$ is observed. This indicates that there is a complete substitution by the dopant ions.

Lattice constants

X-ray diffraction patterns of $Sr_{1-x}RE_xFe_{12}O_{19}$ hexagonal ferrites of the three series under investigation have been obtained using Cu-Kα radiation. The lattice constants 'a' and 'c' were calculated from the diffractograms obtained by the following equation:

$$d_{(hkl)} = \left(\frac{4}{3}\frac{h^2+hk+k^2}{a^2} + \frac{l^2}{c^2} \right)^{-\frac{1}{2}} \quad (4)$$

The variation of lattice constant 'a' and 'c' with composition (x) for the three series prepared with RE = La^{3+}, Nd^{3+} and Sm^{3+} are shown in the Figs. 2 and 3 respectively. It was observed that both 'a' and 'c' decrease continuously with an increase in the amount of rare earth ions substituted for the three series. The observed variation in the lattice constants can be explained on the basis of the relative ionic radii of Sr^{2+} ions and RE^{3+} ions, which are (1.27 Å) for Sr^{2+} and (1.22 Å, 1.16 Å and 1.13 Å) for La^{3+}, Nd^{3+} and Sm^{3+} respectively [24]. Since RE^{3+} ions have ionic radii less than that of the ionic radii of Sr^{2+} ions, the replacement of Sr^{2+} ions by RE^{3+} ions results in a decrease of the unit cell dimensions of the hexagonal lattice. The greater decrease in the lattice constants 'a' and 'c' for Sm^{3+} ions substituted hexaferrites as compared to those for Nd^{3+} ions and La^{3+} ions substituted ones is attributed to the smaller ionic radii of Sm^{3+} ions than those of Nd^{3+} ions and La^{3+} ions.

Scanning electron microscopy

Figs. (4-6) show the SEM images of the fractured surface

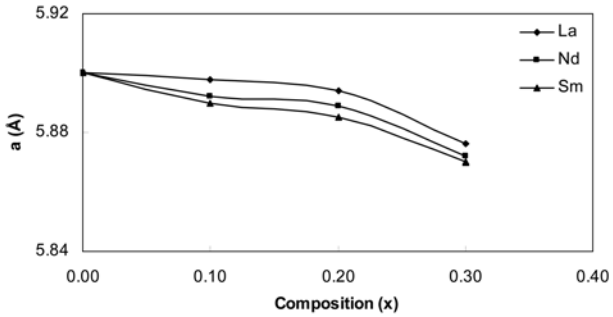

Fig. 2. Variation of lattice constant 'a' with composition (x) for the three series.

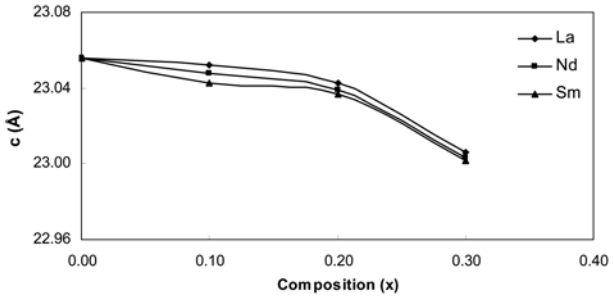

Fig. 3. Variation of lattice constant 'c' with composition (x) for the three series.

of all the samples studied here. Fig. 4(a) is for the undoped sample where as Fig. 4(b-d) is for La-doped samples. Similarly Figs. 5 and 6 are for Nd and Sm-doped samples, respectively. From the SEM micrographs, the average grain size of all the doped and undoped samples was calculated. The variation of the average grain size with composition for all the samples is shown in Fig. 7. It was observed that the average grain size decreased for all the substituted samples. However, this decrease is more in the case of Sm^{3+} substitution. It is observed that the

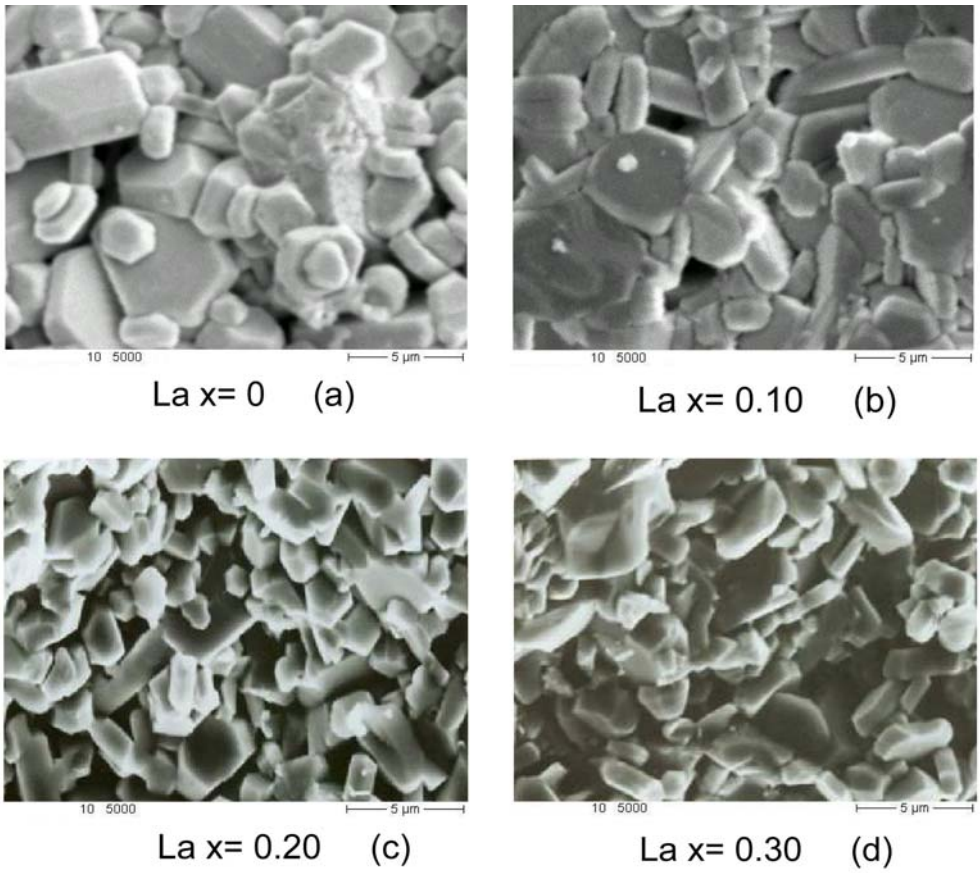

Fig. 4

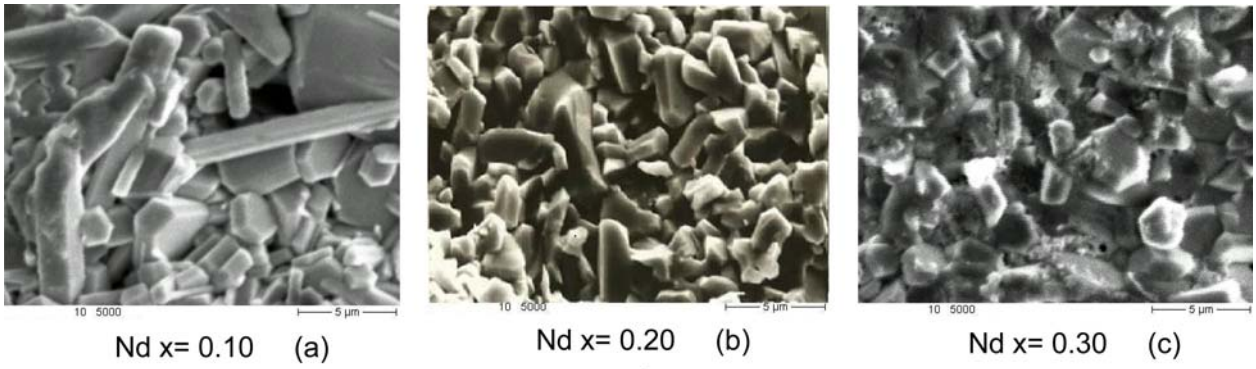

Fig. 5

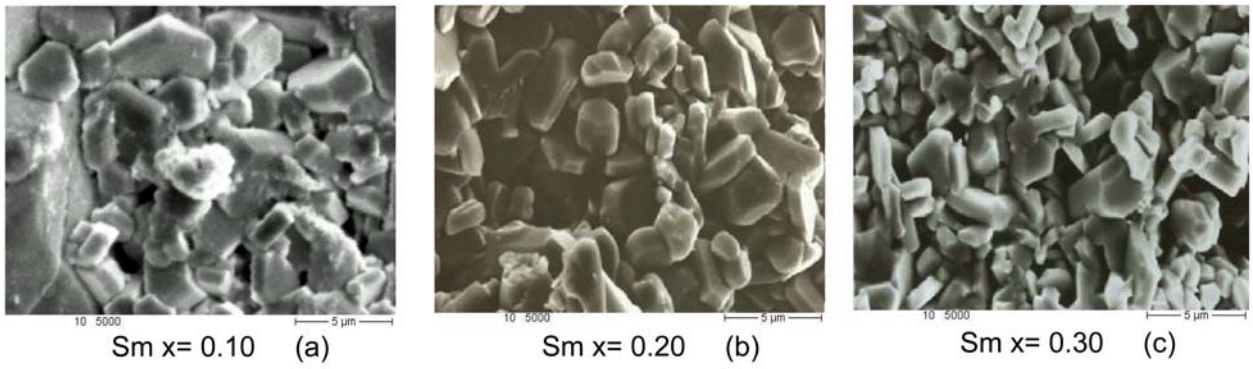

Fig. 6

Figs. (4-6). SEM images for the $Sr_{1-x}RE_xFe_{12}O_{19}$ where RE = La^{3+}, Nd^{3+} and Sm^{3+} with (x = 0 to 0.30).

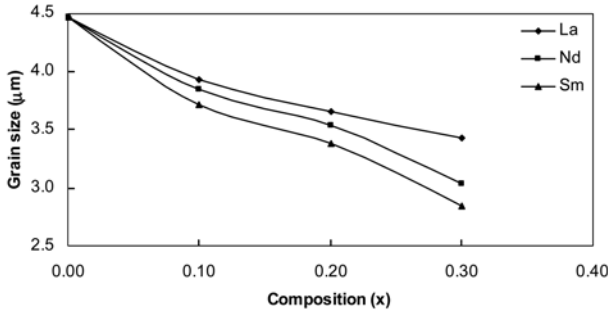

Fig. 7. Variation of grain size with composition (x) for the three series.

decrease in lattice parameters a & c occurs more when the substitution is increased from 0.2 to 0.3. This decrease is because of replacement of parent atoms with dopant atoms in the lattice site. Since the ionic size of Sm is less as compared to the other dopant ions so the unit cell dimension of Sm doped compound is lowest. Doping causes lattice straining in the matrix because of variation in ionic radii. In order to relieve it masses of lower critical size nucleate. Once nucleation occurs its growth is controlled by other factors [25, 26] which depend upon type of interface existing in the system (smooth or rough one). This further depends upon the availability of fraction of the total binding energy which binds an atom in a layer parallel to the plane face to other atoms in the layer. As per Jackson and Hunt model [27] faceted structures can be observed when α parameter is more than 2. We observe hexagonal faceted grains because α for strontium hexaferrite is more than 2. This typical faceted structure of strontium hexaferrite is responsible for better magnetic properties.

Density and porosity

The X-ray density D_x was calculated using the known formula:

$$D_x = \frac{2nM}{\sqrt{3}N_a a^2 c} \tag{5}$$

Here n is the number of molecules per unit cell, N_a is the Avogadro's number per gram mole, 'a' and 'c' are the lattice constants obtained from X-ray diffraction analysis and M is the molecular weight of the sample.

The porosity of the samples was calculated using the relation:

$$P = \left(\frac{D_x - D}{D_x}\right) \times 100\% \tag{6}$$

The composition dependence of the apparent density D, X-ray density D_x and porosity P is shown in Table 1 for the three series. The increase in density with rare earth content can be attributed to the atomic weight and density of the rare earths (138.9, 6.15 g/cm^3 ;144.2, 7.01 g/cm^3 and 150.3, 7.52 g/cm^3) for La^{3+}, Nd^{3+} and Sm^{3+} respectively, which are higher than those of Sr (87.6, 2.54 g/cm^3).

Table 1. X-ray density D_x, Observed density D and Porosity P (%) of $Sr_{1-x}RE_xFe_{12}O_{19}$ where RE = La^{3+}, Nd^{3+} and Sm^{3+} with (x = 0 to 0.30)

RE^{3+}	Composition (x)	D (g/cm^3)	D_x (g/cm^3)	P (%)
La	0	4.20	5.07	17.03
	0.10	4.27	5.10	16.20
	0.20	4.31	5.13	16.02
	0.30	4.37	5.20	15.80
Nd	0.10	4.28	5.11	16.26
	0.20	4.32	5.15	16.03
	0.30	4.39	5.21	15.81
Sm	0.10	4.28	5.12	16.31
	0.20	4.33	5.16	16.07
	0.30	4.39	5.22	15.97

The replacement of RE^{3+} by Sr^{2+} ions in the hexagonal structure leads to a variation in the bonding and consequently interatomic distance and density. The oxygen ions which diffuse through the material during sintering also accelerate the densification of the material. The apparent density of the same sample reflects the same general behavior of the theoretical density D_x. The X-ray density is higher than the apparent density value due to the existence of pores which depend on the sintering condition. This was determined by the Archimedes principle based method. The porosity decreases as the rare earth content increases reflecting the opposite behavior of density. The higher values of X-ray densities for Sm^{3+} ions substituted hexaferrites as compared to those for Nd^{3+} ions and La^{3+} ions substituted ones may be due to the lower value of lattice constants in the former type of substitution.

Frequency variation of AC conductivity, dielectric constant and dielectric loss tangent

The variation of the real AC conductivity σ' as a function of the frequency for all the samples is shown in Fig. 8. This shows that the AC conductivity σ' is generally increased with an increase in the frequency for all the series. The results of AC conductivity can be explained on the basis of the assumption that real AC conductivity consists of two parts [28]:

$$\sigma' = \sigma_{DC} + \sigma_{AC} \tag{7}$$

The first term σ_{DC} is the DC conductivity, which is frequency independent and can be written as:

$$\sigma_{DC} = \sigma_0 \exp(-E/kT) \tag{8}$$

where E is the activation energy for electrical conduction, σ_0 is a pre-exponential constant and k is Boltzmann's constant. The second term σ_{AC} is temperature and frequency dependent and is given by [28, 29]:

$$\sigma_{AC} = B(T)\omega^n(T) \tag{9}$$

where B is the parameter having units of conductivity (Ω^{-1} cm^{-1}) and n is a dimensionless exponent and is temperature and compositional dependent and $\omega = 2\pi f$ is the angular frequency.

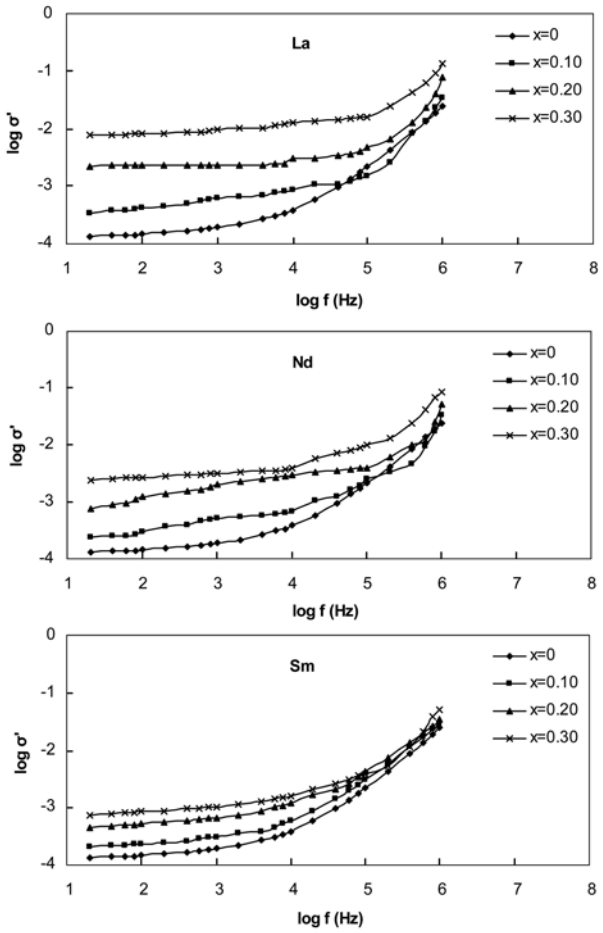

Fig. 8. Variation of the real AC conductivity with frequency for different compositions.

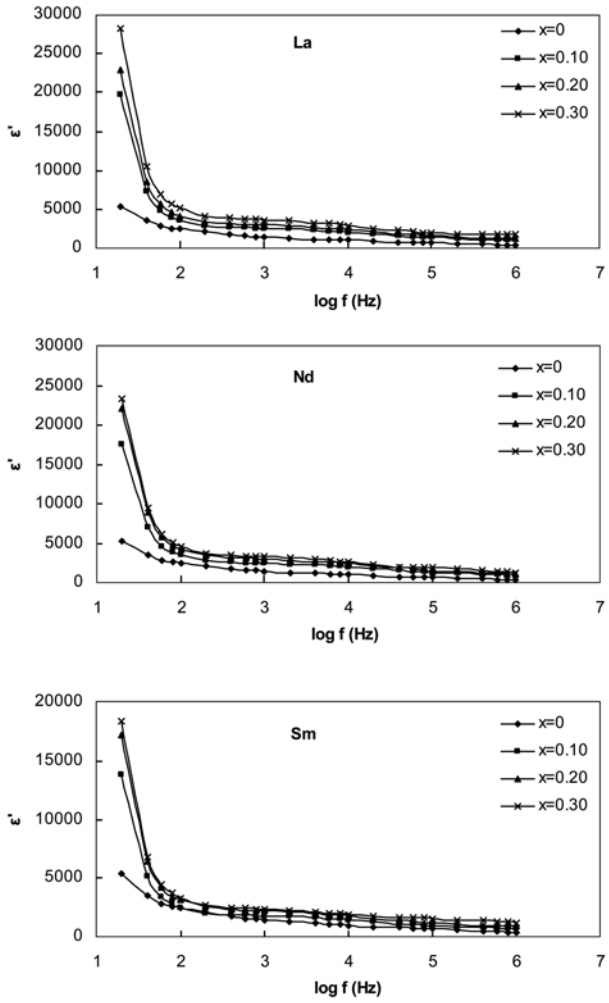

Fig. 9. Variation of the dielectric constant (e) with frequency for different compositions.

The variation of the dielectric constant as a function of frequency for all the samples is shown in Fig. 9. This shows that the value of the dielectric constant decreases regularly with an increase in the frequency. This behavior in Sr-RE ferrites is a normal ferrimagnetic behaviour and has been also confirmed by several investigators [30-33]. More dielectric dispersion is observed in the lower frequency region and it remains almost independent of the applied external field even at higher frequency. The dielectric dispersion observed in the lower frequency region is due to Maxwell-Wagner type interfacial polarization in agreement with the Koops phenomenological theory [30, 34]. Space charge polarization is due to the inhomogeneous structure as suggested by Maxwell and Wagner. The presence of Fe^{2+} ions in an excess amount favours the polarization effects. The decrease in dielectric constant with an increase in the frequency is due to a lag of the hopping frequency of electrons between Fe^{2+} and Fe^{3+} ions against the frequency of the external applied AC field beyond a certain limit of the external field and ultimately it becomes independent of it.

The variation of the dielectric loss tangent as a function of frequency for all the samples is shown in Fig. 10. The dielectric loss tangent value increases as the frequency increases to reach its maximum (peak) value at a certain critical frequency, and then it decreases at higher frequencies. The resonance type behavior in the dielectric loss occurs when the hopping frequency of electron between Fe^{2+} and Fe^{3+} is equal to the frequency of the applied field [35, 36].

Figs. 8 and 9 show the variation of AC conductivity and dielectric constant measured at room temperature as a function of frequency for different compositions (x). The AC conductivity increases with an increase in x. On the other hand, the dielectric constant increases with an increase in x. Similar type of results have been reported in different ferrites [37, 38]. Both the dielectric constant and electrical conductivity are basically electrical properties and it has been recognized that the same mechanism viz. exchange of electrons between Fe^{2+} and Fe^{3+} are responsible for both the phenomena. A strong correlation between the conduction mechanism and dielectric behavior of ferrites has been established by Iwauchi [39] and Rezlescu and Rezlescu [40]. It has been concluded that the electron exchange between $Fe^{2+} \leftrightarrow Fe^{3+}$ results in a local displacement of charges, and this is responsible for polarization

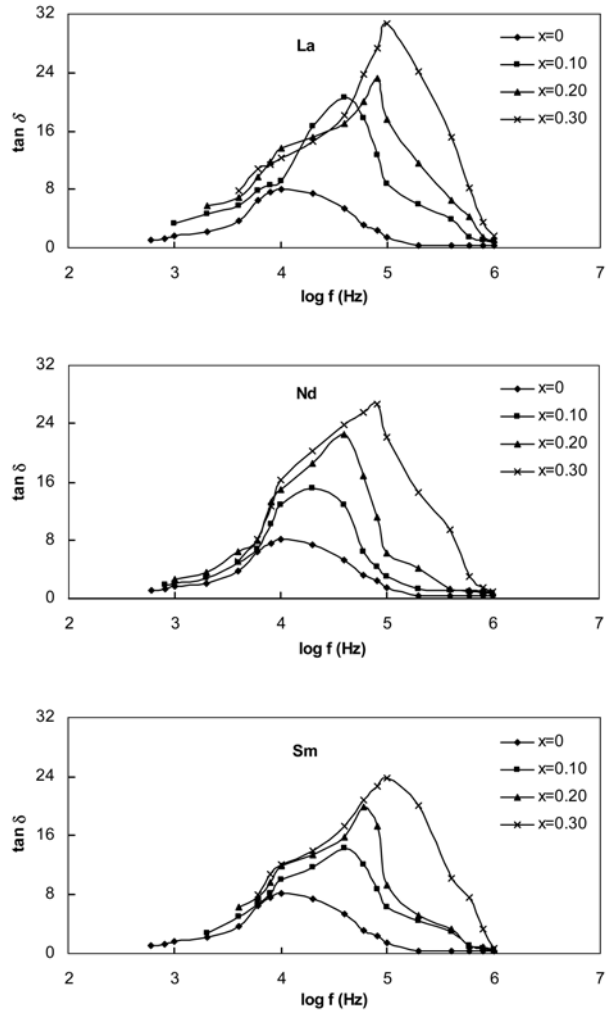

Fig. 10. Variation of the dielectric loss (tan δ) with frequency for different compositions.

in ferrites. The magnitude of the exchange, which also controls the conduction in ferrites, depends upon the concentration of Fe^{3+} / Fe^{2+} ion pairs present on B sites.

The Fe^{2+} ion concentration is a characteristic property of a given material and its value depends on several factors, sintering temperature, sintering atmosphere and annealing time, etc. Some amount of Fe^{2+} ions can also be formed due to the partial reduction of Fe^{3+} ions during sintering. Therefore, the increase of AC conductivity with composition can be attributed to the excess formation of Fe^{2+} ions. Thus, it is the number of ferrous ions on the octahedral sites that play a dominant role in the process of conduction as well as dielectric polarization. At the same substitution content, the AC conductivity (σ_{AC}) and dielectric constant (ε') of La-substituted strontium hexaferrites is larger than those of Nd-doped and Sm-doped hexaferrites due to the larger concentration of Fe^{3+}/Fe^{2+} ion pairs present on the octahedral sites. It has been observed that both the AC conductivity (σ_{AC}) and dielectric constant (ε') increase with an increase in x. The increase is, however, smaller in the case of the Nd and Sm substituted series for x = 0.30. The reason for this might be the existence of an insulating secondary phase on grain boundaries, which may reduce the Fe^{2+} ions on the octahedral sites and also it is true that an extra phase at grain boundaries limits the reduction of Fe^{2+} ions concentration.

Fig. 10 shows the variation of dielectric loss tangent measured at room temperature as a function of frequency for different compositions (x). It shows that tand plot exhibits resonance type behavior for all compositions. The observed peaks are shifted towards higher frequencies accompanied by an increase in the height of the peak with increasing RE ion substitution. The substitution of rare earth ions somehow decreases the distance between Fe^{3+} and Fe^{2+} resulting in a change in hopping frequency. The observed peaks of tan d curves can be explained according to the fact that a strong correlation between the conduction mechanism and the dielectric behavior exist in ferrites [35, 36]. In this case, the peak is expected when the hopping frequency of the electron between Fe^{2+} and Fe^{3+} ions is approximately equal to that of the external applied electrical field. In this case

$$\omega\tau = 1 \tag{10}$$

where τ is the relaxation time of the hopping process and w is the angular frequency of the external field ($\omega = 2\pi f_{max}$). It is also known that the relaxation time t is inversely proportional to the jumping probability per unit time, P, according to the relation [35]:

$$\tau = \frac{1}{2}P \tag{11}$$

So, from equations (10) and (11), it is expected that f_{max} is proportional to P. The shift and increase in height of the peak with increasing RE ion substitution indicates that the jumping probability per unit time, P increases as the RE ion content increases. The increase of jumping probability may be attributed to the increase of ferrous ions on B-sites, which is responsible for the polarization in these ferrites. The dielectric loss (tan δ) is observed to be a maximum in the case of La-substituted strontium hexaferrites. These losses in ferrites are generally reflected in the resistivity measurements. Materials with a high resistivity (low conductivity) exhibit low dielectric losses and vice versa [41]. An increase of loss tangent values in RE-substituted Sr hexaferrites confirms the increase in conductivity [42, 43] supporting the Verway conduction mechanism [44].

Magnetic measurements

Fig. 11 shows the variation of magnetization (M_s) and remanence (M_r) with composition for all the series. It is shown in Table 2 that the values of magnetzation (M_s) and remanence (M_r) decrease with increasing substitution. For the same substitution content, the values of M_s and M_r of La-doped strontium hexaferrites are higher than those of Nd-doped and Sm-doped samples. The decrease in

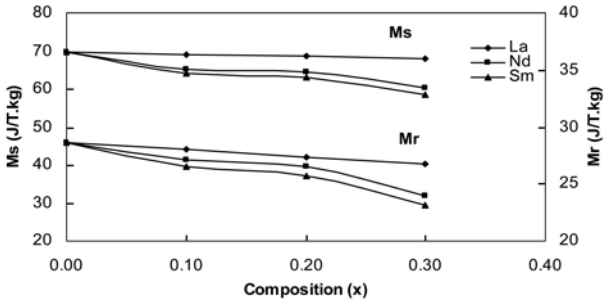

Fig. 11. Variation of the magnetization (M_s) and remanence (M_r) with composition x.

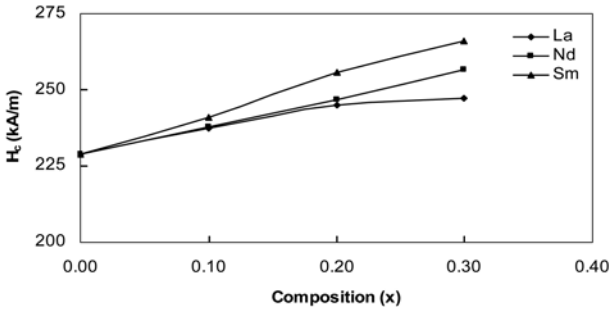

Fig. 12. Variation of the coercive field (H_c) with composition x.

Table 2. Effects of rare-earth ions on the magnetic properties of $Sr_{1-x}RE_xFe_{12}O_{19}$ (with x = 0 to 0.30)

RE^{3+}	Composition (x)	M_s (J/T.kg)	M_r (J/T.kg)	H_c (kA/m)
La	0	69.7	28.6	228.7
	0.10	69.2	28.1	237.5
	0.20	68.7	27.4	244.7
	0.30	68.1	26.8	247.0
Nd	0.10	64.1	26.6	237.9
	0.20	63.3	25.7	246.8
	0.30	58.5	23.2	256.7
Sm	0.10	64.1	26.6	240.7
	0.20	63.3	25.7	255.6
	0.30	58.5	23.2	266.1

M_s and M_r values of all the series may be due to magnetic dilution with a change of the Fe^{3+} (high spin) valence state to Fe^{2+} (low spin) state on a site by substitution of the Sr^{2+} sites with RE^{3+} ions and the existence of spin canting promoting reduction of superexchange fields [15].The Fe^{3+}-O^{2-}-Fe^{3+} exchange interaction is disrupted and weakened by Fe^{2+} ion canted spins, which could be produced by substitution of the rare earth ions into the hexaferrite [15, 17]. Moreover the decrease in M_s and M_r were found to be a maximum at a composition of x = 0.30 in the case of the Nd and Sm- substituted strontium hexaferrites. This decrease could be due to the existence of nonmagnetic phases observed for higher rare earth concentrations in the case of Nd and Sm substitutions. It seems that the main role of these nonmagnetic phases are to isolate Sr-ferrite particles from each other, thus reducing exchange interaction between them and are known to have a detrimental effect on M_s and M_r.

Fig. 12 shows the variation of coercive field (H_c) with composition for all the series. It shows that the value of the coercive field (H_c) increases with an increase in the concentration of rare earth substitution. The increase in H_c for all the series can be attributed to an enhancement of the magnetocrystalline anisotropy [45] with anisotropic Fe^{2+} ions locating on a 2a site and the grain size reduction which is usually found with rare earth substitutions, which is evident in the SEM micrographs [46, 47]. However for the same substitution content, the H_c value of La-substituted strontium hexaferrite is correspondingly smaller than those of Nd-doped ferrites and Sm-substituted ferrites due to the smaller magnetocrystalline anisotropies and larger grain size. This suggests that the effect of Fe^{2+} anisotropy on the 2a site in the Nd and Sm-doped samples could be stronger than those in La-doped samples [46, 47]. Table 1 shows the effect of doping on the sintered density. The sintered density is observed to increase with an increase in the dopant content. This also depends upon particle size and their distribution [25]. The structural features indicate a hexagonal faceted structure with varying grain size. The increase in coercivity (Hc) with an increase in density depends upon the oxidation of the grains and their size.

Conclusions

M-type hexagonal ferrites $Sr_{1-x}RE_xFe_{12}O_{19}$ samples where RE = La^{3+}, Nd^{3+} and Sm^{3+} with (x = 0 to 0.30) were prepared by a ceramic processing technique. The increase in AC conductivity with frequency has been explained on the basis of Koops Model, whereas the dielectric constant and dielectric loss tangent has been explained with the Maxwell-Wagner type interfacial polarization in agreement with the Koops phenomenological theory. Out of the three series prepared, La-substituted strontium hexaferrites showed the largest variation in AC conductivity, dielectric constant (ε') and dielectric tangent loss (tan δ) with an increase in frequency. This variation may be attributed to the excess formation of Fe^{2+} ions which play a dominant role in the process of conduction as well as in dielectric polarization. It is found that the values of magnetization (M_s) and remanence (M_r) decrease with an increase in the rare earth substitution for all the series. Such a decrease may be due to presence of nonmagnetic phases at higher rare earth concentrations in the case of Nd and Sm substitutions and both the magnetic dilution and spin canting ultimately promotes reduction in superexchange interactions. The enhancement of H_c could be due to higher magnetocrystalline anisotropy, where Fe^{2+} ion anisotropy on the 2a site may be dominant in all the hexaferrite series.

References

1. J. Smit and H.P.J. Wijn, “Ferrites: Physical properties of

ferrimagnetic oxides in relation to their technical Applications" (Eindhoven: N.V. Philips Gloeilampenfabrickon, 1959).
2. E.E. Riches, in "Ferrites" (Mills, Boon Technical Library, Boon, London, 1972).
3. J. Kracch and M.H. Grant, in "Encyclopedia of chemical Technology" (Wiley 4th edition, 1993).
4. H. Yamamoto, M. Nagakura and H. Terada, IEEE Trans. Magn. 26 (1990) 1144-1148.
5. J.F. Wang, C.B. Poton and I.R. Harris, J. Magn. Magn. Mater. 234 (2001) 233-240.
6. H. Kojima, in "A Handbook on the Properties of agnetically ordered substances" (Amsterdam, North-Holland, 1982).
7. C.S. Kim, S.W. Lee and S.Y. An, J. Appl. Phys. 87 (2000) 6244-6246.
8. A.L. Stuijits, Trans. Brit. Ceram. Soc. 55 (1956) 57-74.
9. F.J.A. Den Broendner and P.E.C. Franken, Adv. Ceram. 1 (1985) 494-498.
10. G. Turilli, F. Licci, A. Paoluzi and T. Besajni, IEEE Trans. Magn. 24 (1988) 2146-2149.
11. G. Turilli and A. Paoluzi, IEEE Trans .Magn. 24 (1988) 2865-2867.
12. G. Turilli and F. Licci, J. Magn. Magn .Mater. 75 (1988) 111-114.
13. S. Rana, H. Krishna, K.N. Rai and K.A. Narayan, Jpn. J. Appl. Phys. 28 (1989) 604-608.
14. G.K. Thompson and B.J. Evans, J. Appl. Phys. 29 (1994) 1944-1949.
15. X. Liu, W. Zhong, S. Yang, Z. Yu, B. Gu and Y. Du, Phys. Stat. Sol. (A) 193 (2002) 314-319.
16. L. Lechevallier, J.M. Le Breton, A. Morel and J. Teillet, J. Alloys Comp. 359 (2003) 310-314.
17. X. Liu, W. Zhong, S. Yang, Z. Yu, B. Gu and Y. Du, J. Magn. Magn. Mater. 238 (2002) 207- 214.
18. M.W. Pieper, F. Kools and A. Morel, Phys. Rev. B, 65 (2002)184-189.
19. F. Kools, A. Morel, R. Grossinger, J.M. Lebreton and P. Tenaud, J. Magn. Magn. Mater. 242 (2002) 1270-1276.
20. A.M. Abo El Ata and M.A. Ahmed, J. Magn. Magn. Mater. 208 (2000) 27-36.
21. H. Ismael, M.K. El Nimr, A.M. Abou El Ata, M.A. El Hiti, M.A. Ahmad and A.A. Murakhowski, J. Magn. Magn. Mater. 150 (1995) 403-408.
22. A. Singh, S.B. Narang, K. Singh, P. Sharma and O.P. Pandey, Eur. Phys. J. Appl. Phys. 33 (2006) 189-193.
23. S.B. Narang, A. Singh and K. Singh, J. Ceram. Process. Res.8[5] (2007) 347-351.
24. S. Ounnukad, Solid State Commun. 138 (2006) 472-475.
25. P. Sharma, A. Verma, R.K. Sidhu and O.P. Pandey, Magn. Magn. Mater. 307 (2006) 157-164.
26. A.A. Sattar, A.H. Wafik, K.M. El- Shokrofy and M.M. El Tabby, Phys. Stat. Sol. (A) 171 (1999) 563-569.
27. K.A. Jackson, D.R. Uhlmann and J.D. Hunt, J. Crystal Growth 1 (1967) 1-36.
28. A.K. Jonscher, in "Dielectric Relaxation in Solids" (Chelsea Dielectric Press, London, 1983).
29. M.F. Mostafa, M.M. Abd. El Kader, A.S. Atallah and M.K. El Nimr, Phys. Stat. Sol. (A) 135 (1993) 549-556.
30. C.G. Koops, Phys. Rev. 83[1] (1951) 121-124.
31. D. Ravinder, P. Vijaya and B. Reddy, Mater. Lett. 57 (2003) 4344-4350.
32. A.M. Shaikh, S.S. Belled and B.K. Chougule, J. Magn. Magn. Mater. 195 (1999) 384-390.
33. B.R. Kumar and D. Ravinder, Mater. Lett. 53 (2002) 437-440.
34. K.W. Wagner, Ann. Phys. 40 (1973) 817-819.
35. M.B. Reddy and P.V. Reddy, Appl. Phys. (UK) 24 (1991) 975-981.
36. S.C. Watawe, B.D. Sarwede, S.S. Bellad, B.D. Sutar and B.K. Chougule, J. Magn. Magn. Mater. 214 (2000) 55-60.
37. P. Kishan and N. Kumar, J. Magn. Soc. Jpn. 22 (1998) 21-24.
38. S.S. Bellad and B.K. Chougule, Mater. Chem. and Phys. 66 (2000) 58-63.
39. K. Iwauchi, Jpn. J. Appl. Phys. 10 (1971) 1520-1528.
40. N. Rezlescu and E. Rezlescu, Phys. Stat. Sol. (A) 23 (1974) 575-582.
41. C.B. Kolekar, P.N. Vasambekar, S.G. Kulkarni and A.S. Vaingankar, J. Mater. Sci. 30 (1995) 5784-5788.
42. N.J. Ali J. Rahman and M.A. Showdhaury, J. Jpn. Appl. Phys. 39 (2000) 3378-3381.
43. A.Y. Lipare, P.N. Vasambekar and A.S. Vaingankar, Phys. Stat. Sol. (A) 196 (2003) 372-378.
44. E.J.W. Verway, P.M. Haaijman, G.M. Romeyn and F.C. Vas Oosterhout, Philips Res. Rep. 9 (1954) 428-438.
45. L. Lechevallier, J.M. Le Breton, J.F. Wang and I.R. Harries, J. Magn. Magn. Mater. 269 (2004) 192-196.
46. C. Sauer, U. Kobler, W. Zinn and H. Stablein, J. Phys. Chem. Solids 39 (1978) 1197-1201.
47. J. Dho, E.K. Lee, Y.Y. Park and N.H. Hur, J. Magn. Magn. Mater. 285 (2005) 164-168.